To appear in Journal of Geophysical Research (Final, 01/02/2001)

Plasma sheet access to the inner magnetosphere

R. H. W. Friedel, H. Korth, M. G. Henderson and M. F. Thomsen

Los Alamos National Laboratory, Los Alamos, New Mexico

J. D. Scudder

Department of Physics and Astronomy, University of Iowa, Iowa City

Abstract. We present here plasma data from the Polar HYDRA instrument giving comprehensive coverage of the inner magnetospheric region from $L \sim 2$ outward. Data is projected to an equatorial reference plane yielding a global view of the inner extend of the plasma sheet. We determine the inner boundary for plasma sheet electrons and ions in the μ range 0.05 – 50 $\mathrm{eV\ nT^{-1}}$ and we compare these to the predicted Alfvén boundaries as a function of the geomagnetic activity index Kp. In general, the simple conventional drift paradigm is shown to be globally consistent with the averaged data in the inner magnetosphere, with electrons adhering better to the predicted boundaries than ions. The data are further compared to the geosynchronous slice as measured by the Los Alamos Magnetospheric Plasma Analyzer (MPA) which measures the crossing point of the Alfvén boundaries at geosynchronous altitudes with much better statistical resolution than Polar. Integral to the drift model used is an assumption about the form of the global electric field. The agreement with data validates the simple corotation and convection electric field used and shows that this model describes well the average transport for a wide range of geomagnetic activity and over a large part of the inner magnetosphere.

1. Introduction

The plasma sheet is an important source region for much of the hot plasma observed in the inner ($L < 8$) magnetosphere. This is true, in general, during quiet times (steady or "background" convection) and even more important for disturbed times such as magnetic storms and substorms, when, in general, hot plasma has temporally limited access to the innermost magnetospheric regions.

Detailed simulations by *Birn et al.* [1997, 1998] and *Toivanen et al.* [1999], which model the injection of energetic particles at substorm onset, all depend on some near-Earth reservoir in the plasma sheet, from which particles can be moved from open to closed drift paths. The same mechanism on a grander scale is invoked for storm time particle injections and increases of the ring current, which can capture large portions of the near-Earth plasma sheet onto closed drift paths. For this reason many ring current or inner magnetospheric transport codes [*Jordanova et al.*, 1998; *Bourdarie et al.*, 1997] use the plasma sheet as an outer boundary condition (often based on Los Alamos geosynchronous data).

All the above dynamics depend critically on where and when particles have access to the inner magnetosphere. In this study we expand on previous work done by *Korth et al.* [1999] and *Maurice et al.* [1998]. Both these studies examined the plasma environment at geosynchronous orbit in a statistical sense, with *Korth et al.* [1999] expanding this to cover all Kp conditions. *Korth et al.* [1999] also applied the conventional particle drift paradigm to their observations and were able to show that a simple parameterization of the convection electric field strength with Kp, together with the concept of Alfvén boundaries, was exceptionally successful in ordering their data and in understanding the average plasma sheet access to geosynchronous orbit during both quiet and disturbed times.

This work expands the results of both these previous studies to cover the entire inner magnetosphere by using data

from the Polar HYDRA instrument. Apart from showing excellent agreement with the geosynchronous "slice" examined by *Korth et al.* [1999], this study is able to show that the same models and assumptions used in that study successfully order the plasma sheet access to the inner zone in a global sense. We thus expand our ability to examine the validity of the electric field models used in determining the theoretical particle access boundaries (Alfvén boundaries). Low μ drifts are controlled chiefly by the electric field: Fitting good boundaries to data then shows the global validity of the electric field models used, albeit in an average, statistical sense.

2. Particle Drift

This work uses the (U,B,K) formulation introduced by *Whipple* [1978]. This framework for analyzing particle drift trajectories and access to the inner magnetosphere has also recently been used by *Sheldon and Spence* [1997], *Whipple et al.* [1998], and *Korth et al.* [1999]. The (U,B,K) formulation defines a particle's total energy in terms of the electric potential and the magnetic field:

$$W_{\rm tot} = qU + \mu B_m \ , \tag{1}$$

where q is the particle's charge, μ is the magnetic moment, and U and B_m represent the electric potential and the magnetic field strength at the mirror point, respectively. In this coordinate system all particle trajectories become simple straight lines with a slope proportional to the particle's magnetic moment:

$$\Rightarrow \frac{\partial U}{\partial B_m} = -\frac{\mu}{q} \ . \tag{2}$$

The quantity K is proportional to the true longitudinal invariant J and is defined as

$$K(\mathbf{r}) = \oint [B(\mathbf{r}) - B(s)]^{1/2} ds \ , \tag{3}$$

where s is the distance along the field line going through point **r**.

Assuming an equatorial pitch angle of $90^{\rm o}$ for the model, the K coordinate may be omitted and B_m may be replaced by the equatorial magnetic field strength. We will show in section 4.2 that this is a reasonable assumption to make: All the calculations of Alfvén layers for data comparison in this paper are for $K = 0$.

For the calculations of Alfvén layers we use a simple dipole for the magnetic field model, since this is a very good approximation for the inner magnetosphere in a statistical sense. We use an electric potential configuration due to superposition of a shielded cross-tail electric field with a corotation electric field [*Volland*, 1973; *Stern*, 1975]:

$$U = -\frac{a}{r} - br^{\gamma} \sin(\phi) \ , \tag{4}$$

where r is the distance from the center of the Earth, ϕ is the magnetic local time referred to from noon,γ is the shielding factor, and $a = 92.4$ kV R_E^{-1} is the corotation constant. The convection electric field b can be parameterized by the magnetospheric activity level represented by the Kp index; for a shielding factor of $\gamma = 2$ this dependence has been expressed as [*Maynard and Chen*, 1975]

$$b = \frac{0.045}{(1 - 0.159Kp + 0.0093Kp^2)^3} \ , \tag{5}$$

where units are $\rm kV\ R_E^{-2}$. In this formulation, particle fluxes should be organized by the boundaries between the open and closed drift trajectories. These boundaries are known as the Alfvén layers, which can be simply identified as straight lines tangent to the potential bounding curves in the (U, B, K) space.

2.1. Components of Drifts

In the discussion that follows it will be useful to split up the overall particle drifts discussed in section 2 into their components. This will be useful in understanding the different dynamics of ions and electrons.

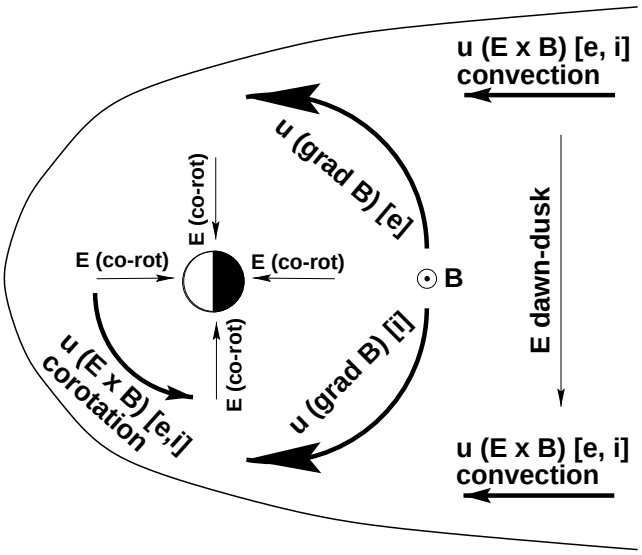

Figure 1. Components of particle drift u in the magnetosphere.

Figure 1 shows a simplified schematic of the equatorial plane. Large-scale electric fields (dawn-dusk and corota-

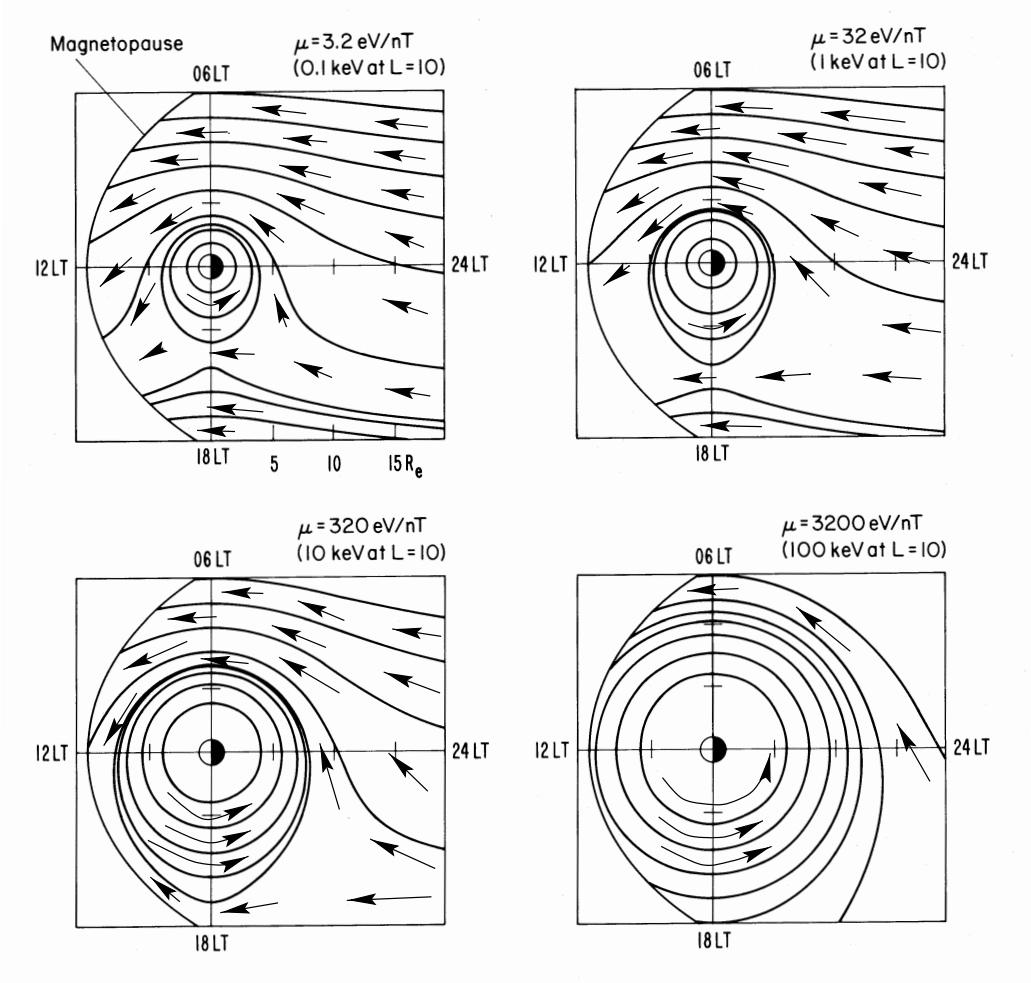

Figure 2. Electron drift trajectories for four μ values in the equatorial plane with arrows showing the direction of drift.

tion) and their associated $E \times B$ drifts u are shown (sunward for dawn-dusk electric field, eastward for corotation electric field); they are in the same direction for electrons and ions. The magnitudes of these drifts are independent of energy and depend only on the electric and magnetic fields.

Particles further undergo gradient and curvature drifts owing to the nonhomogeneous magnetic field strength. These drifts are in the opposite direction for electrons (eastward) and ions (westward). The magnitudes of these drifts are dependent on energy.

The total drift of any particle is the combination of all the above drifts. In general, lower-energy particles have their drifts dominated by the "electric field drifts" while the highest-energy particles are dominated by the "magnetic field drifts." For a more detailed discussion of these drifts, see *Roederer* [1970].

The combined drifts for electrons are shown in Figure 2 (taken from *Lyons and Williams* [1984]) for a range of μ. In each graph in Figure 2, regions of open and closed drift trajectories can be identified. Open drift trajectories transport fresh plasma sheet material from the magnetotail in toward the Earth and around it. Near the Earth the drift trajectories form closed orbits that are not accessible by the plasma sheet population arriving from the tail. Particles on the closed drift trajectories can complete many orbits around the Earth. The boundary separating these two regions is the Alfvén layer.

2.2. Use of Alfvén Layer Concept

We can use the drift access argument to "predict" the regions and energies which should be populated by significant flux levels. For the lowest-energy, cold plasma population (< 20 eV) the predominant source is the ionosphere. These fluxes can only become significant on closed drift shells, where particles are trapped for many orbits and fluxes can build up. Particles on open drift trajectories are lost on the timescale of hours and cannot build up. Thus, for this energy range we would expect the Alfvén layer to be a bound-

ary between high fluxes on the earthward side and low fluxes elsewhere.

For higher energies (> 100 eV) the main source is the plasma sheet, and the access is by convection and gradient/curvature drift. For this energy range we would expect the Alfvén layer to be a boundary between low fluxes on the earthward side and high fluxes elsewhere. During disturbed, stormtime conditions when the convection electric field strength changes, the Alfvén layer position can change by several R_E on short timescales: These higher-energy particles can be captured onto closed drift shells at that time. This is the major mechanism leading to the stormtime buildup of the ring current [*Williams*, 1987; *Korth et al.*, 2000, accepted]. However, since loss processes are active at all times (for electrons, particle precipitation by scattering into the loss cone through wave-particle interaction [*Abel and Thorne*, 1998a, b]; for ions, coulomb scattering and charge exchange [*Fok et al.*, 1991]), these trapped populations cannot persist over time.

The same loss mechanisms also act outside the Alfvén layer on particles on open drift shells. The longer a given particle is exposed to these loss mechanisms, the higher the probability of its loss. This leads to the lower particle fluxes observed on the dayside, for both electrons and ions. This loss gap is expected to become wider in local time for lower-energy particles which drift slower and spend more time subject to these losses.

3. Mission and Instrumentation

The Polar spacecraft has an elliptical orbit $\sim 1.8 - 9\ R_E$ at 86^o inclination. The spacecraft traverses the inner region field lines four times each orbit, at different magnetic local times (MLT's) and at different magnetic latitudes. All MLT's are covered within half a year, and the field lines threading Polar's orbit cover virtually the whole of the magnetosphere. Figure 3 shows the equatorial crossing points of the field lines threading the position of Polar for one whole year (1997). For more details on the field line tracing used here, see section 4.1.

Polar has been operating continuously for over 4 years. While most attention has been on boundary crossings and examinations of the cusp, Polar also offers a continuing coverage of the inner magnetosphere. Here we are interested in plasma sheet particle access to the inner magnetosphere, and we restrict ourselves to $\pm 15\ R_E$ in GSM X and Y in the equatorial plane. For this study we use particle data from the HYDRA plasma instrument [*Scudder et al.*, 1995] for the period March 1996 to December 1998. HYDRA measures the full ion and electron distribution functions at subspin resolution (< 6 s) for the energy range of 20-20,000 eV. We further use data from the Magnetic Field Instrument (MFI) [*Russell et al.*, 1995] to calculate in situ μ values for the locally mirroring population (see section 4.2).

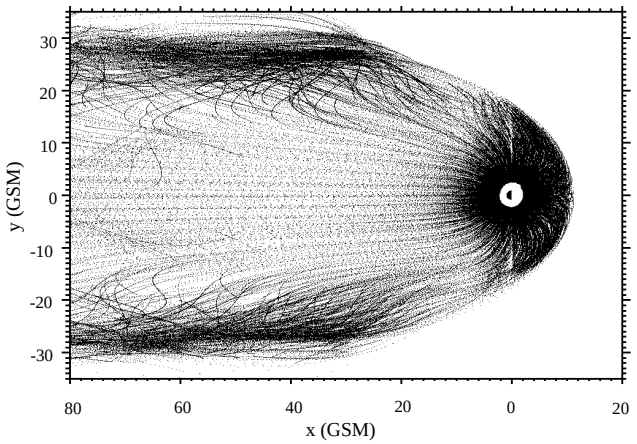

Figure 3. Equatorial crossings in GSM coordinates of the field lines threading Polar's orbits during 1997.

4. Data Analysis

To "see" the global access of plasma sheet particles to the inner magnetosphere we need to establish a common reference, both in physical space and in invariant space. Particle trajectories have commonly been analyzed in the equatorial plane, as is the case for this paper. The physical quantity conserved by drifting particles is their first adiabatic invariant μ. We thus project all Polar measurements along field lines to the geomagnetic equator at constant μ.

4.1. Equatorial Field Line Crossings

Plate 1 shows the data coverage in the equatorial plane for the period of study. The bin size for accumulating data is $0.5\ R_E \times 0.5\ R_E$, and the coverage data is for a μ value of $2\ \mathrm{eV\ nT^{-1}}$ (using the measured B), which is covered by HYDRA throughout a Polar orbit (see Figure 5).

We use here the Tsyganenko 87 Kp-dependent magnetic field model as the external magnetic field and a dipole + tilt for the internal field. The choice of model was dictated by the speed of execution, as we needed to calculate the field lines threading each Polar position (at 1-min time resolution). Inclusion of the International Geomagnetic Reference Field (IGRF) internal model would have severely increased the execution time, and for the majority of the region covered by Polar ($> 2\ R_E$) the higher-order terms of the IGRF expansion can be neglected.

For each satellite position we traced the field line to the equatorial plane using magnetic field model and Kp for that

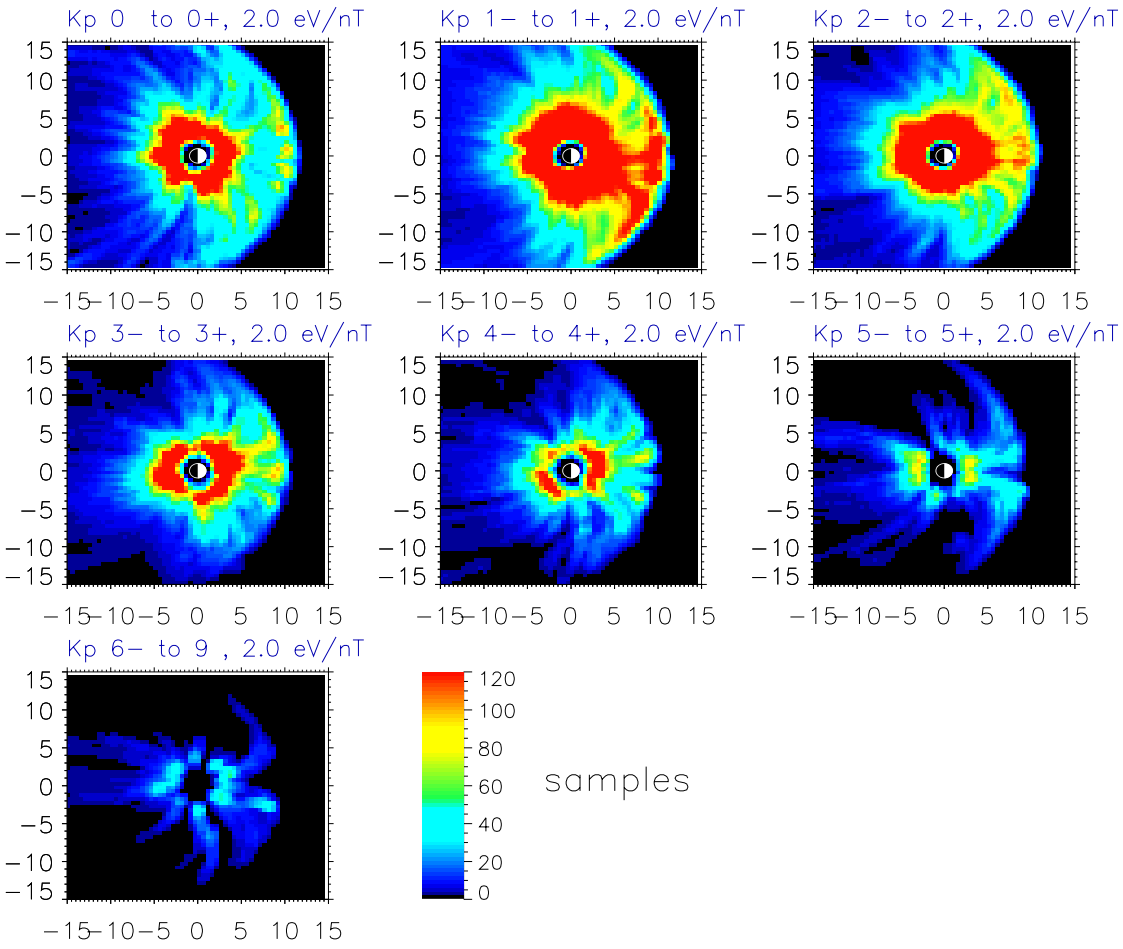

Plate 1. Data coverage in the equatorial plane for 2 eV nT^{-1} particles.

period. Inclusion of this Kp dependence is essential, as our model/data comparisons are parameterized by Kp. To take account of the nightside "hinge region" (the region where the magnetotail transition to the inner, more dipolar magnetosphere occurs), we use two definitions of "equatorial plane." On the dayside the equatorial crossing point of the field line is taken as the point where the field line crosses the GSM $z = 0$ plane. On the nightside the equatorial crossing is taken at the point where the magnetic field direction is perpendicular to the radial direction ($\vec{B} \cdot \Delta|\vec{B}| = 0$). This definition is equivalent to the $B_{\min}$ point but more sensitive, since for quite a range of magnetic latitudes near the equator, B is very close to $B_{\min}$ (this gets worse with radial distance). The use of the GSM $z = 0$ plane on the dayside was motivated simply by computational speed and the fact that in this region it is a good approximation.

Plate 1 is in the same format as that used throughout for the presentation of data here. Data are binned according to Kp ranges, summing ranges together to obtain better statistics and to conform to the Kp ranges used in the magnetic field model for the tracing, which are limited to integer values. All the highest Kp data are binned together since the frequency of occurrence is very low for $Kp > 6$. The correspondence between model input and the "real" Kp used to divide the data is shown in Table 1.

The x and y ranges for each plot in Plate 1 are in GSM coordinates. The color intensity scale indicates the number of samples that contribute to each $0.5\ R_E \times 0.5\ R_E$ bin (values > 120 are assigned red). Coverage in the inner magnetosphere is uniformly high, and up to 10 R_E the number of samples remains generally above 35. Since for the μ ranges considered here the Alfvén layer is generally within 10 R_E, we are sure that we have adequate samples to investigate that boundary. Outside of 10 R_E the number of samples is

Table 1. Correspondence Between T87 Kp Input and Data Binning Ranges

Kp Type	Kp Ranges			
	a	b	...	f
T87 Kp[a]	0	1	...	5
Data Kp	0 – 0+	1- – 1+	...	5- or up

[a]T87 takes only integer Kp in the range 0–5 as input.

low enough so that individual events can dominate the average flux observed in a given bin. Data coverage reflects the distribution of Kp for the study period. In the inner zone ($< 10\ R_E$), coverage remains fairly uniform up to the Kp $4-$ to $4+$ range.

The high number of samples near the dayside magnetopause is a function of the critical mapping of field lines near the cusp, where field lines close together in the cusp can map to widely different regions downtail. This magnifies any differences between the model field lines and the real field lines, making the mapping unreliable in that region.

4.2. Comparison by First Adiabatic Invariant

In the simple drift scenario presented in section 2 all particles with a given value of the first adiabatic invariant μ drift together. We can calculate μ at any point along the Polar orbit using the locally mirroring (90^o pitch angle at mirror magnetic latitude λ_m) particles at energy E_k and the in situ magnetic field magnitude B:

$$\mu = \frac{mv_\perp^2}{2B} = \frac{E_k}{B}\ . \qquad (6)$$

Since μ is conserved along a field line (and everywhere else), this represents the equatorial μ of the particle. However, the same μ measured at various magnetic latitudes (λ) represents particles with different pitch angles α_{eq} (or different K in the U, B, K formulation) and different energies at the equator. Most of the Alfvén boundaries for μ considered in this study lie between 4 R_E and geosynchronous (6.6 R_E). For the period of this study, the Polar satellite crosses the field lines that connect to the equatorial plane at 4 R_E at magnetic latitudes of 0^o to $\sim \pm 25^o$, and geosynchronous (6.6 R_E) at magnetic latitudes of $\sim \pm(25^o - 40^o)$.

Table 2 shows the values of equatorial pitch angle related to the latitude of their mirror point along a field line (90^o pitch angle) and the corresponding value of K for these two values of R_E. K starts exceeding 100 for the region near geosynchronous and beyond. Particles with different values of K (equatorial pitch angle) have slightly different drift paths for the same μ. This, in turn, yields slightly different Alfvén boundaries. In Figure 4 we show a sample of the variation of the Alfvén boundary for $\mu = 10\ eV/nT$ electrons for the values of K shown in Table 2.

Table 2. K Values used in Figure 4 With Equatorial Pitch Angles and Mirror Latitude

K, $\sqrt{(nT)}R_E$	At 6.6 R_E		At 4.0 R_E	
(U, B, K)	α_{eq}, deg	λ_m, deg	α_{eq}, deg	λ_m, deg
0	90	0	90	0
5	72	9	74	8
10	66	12	68	11
50	44	24	48	21
100	33	31	37	28
250	20	41	23	39

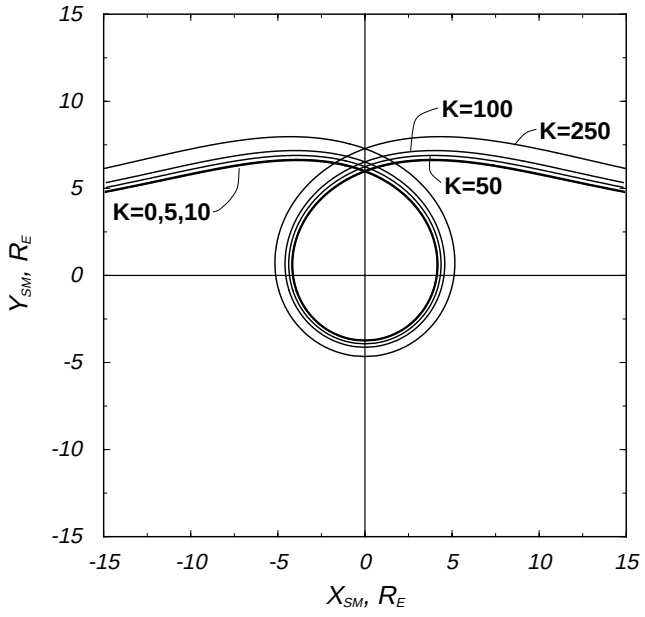

Figure 4. Variation of the Alfvén boundary for 10 eV nT^{-1} electrons, $Kp = 4.5$, $\gamma = 2$, for several K (see Table 2).

In general, for equatorial pitch angles up to 25^o degrees away from 90^o (K up to 10) the Alfvén boundaries are identical, and the particles stay within 10^o of the magnetic equator. Beyond that, as particles traverse more and more of the field line each bounce, the Alfvén boundary is shifted noticeably outward. This change becomes progressively larger as the particles become more field aligned. For the present

study, especially at the higher Kp values, the theoretical Alfvén boundaries lie in an area for which the K value for the mapped Polar data is below 100, and as can be seen from Figure 4 the variation of the Alfvén boundaries for $K = 0 - 100$ is small, of the order of the resolution of our data binning ($0.5\ R_E \times 0.5\ R_E$).

In this study the mapped data along a given Alfvén boundary never has a constant K, as the average magnetic latitude of Polar changes. However, as we can see from Figure 4, for the region from near geosynchronous inward this is of little consequence as the variation of the Alfvén boundaries with K is small in that region. Since the general shape of the Alfvén boundaries is preserved as a function of K, and we are in principle unable to pick a single K for a boundary, we perform all calculations of the Alfvén boundaries for $K = 0$, and we expect this boundary to be representative for all observed K near and within geosynchronous altitude. This assumption, at least for electrons, is corroborated by the good data/model fit presented later (section 5).

Polar samples the particle distribution over a large range of magnetic latitudes and magnetic field strengths, thus the range of μ sampled along the orbit changes constantly. However, HYDRA's energy range and the range of magnetic field strengths encountered during an orbit allow for an almost complete coverage for a range of μ from 0.05 to 50.0 $\mathrm{eV\ nT^{-1}}$ (Figure 5).

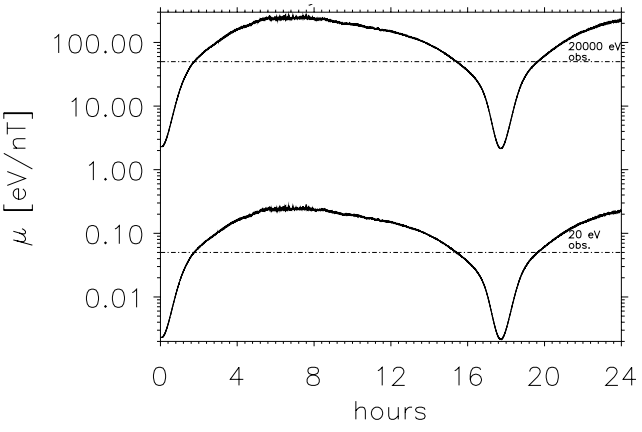

Figure 5. Variation of μ over a sample Polar orbit on February 22, 1998. Lower line shows the variation for the 20 eV channel, and the upper line shows the variation for the 20 keV channel. The values between the dashed horizontal lines are the range of μ chosen for this study.

At each Polar location we convert the measured spectrum to μ and then interpolate to a fixed set of 10 logarithmically spaced μ values. Table 3 shows the μ chosen and their corresponding approximate energy values at various equatorial R_E.

Table 3. Correspondence Between μ Values and Equivalent Particle Energy atSseveral R_E

μ, $\mathrm{eV\ nT^{-1}}$	eV, R_E=4	eV, geo	eV, R_E=10
0.05	25	6.25	1.5
0.1	50	12.5	3.0
0.2	100	25.0	6.0
0.5	250	62.5	15
1.0	500	125	30
2.0	1000	250	60
5.0	2500	625	150
10.0	5000	1250	300
20.0	10000	2500	600
50.0	25000	6250	1500

We make no attempt here to transform the in situ flux magnitude to the equator. For the current work the absolute magnitude of equatorial plasma sheet fluxes are of less importance, as we can use steep gradients in the observed mapped particle distributions in the equatorial plane to determine the Alfvén boundaries.

5. Observations

The results of our analysis are shown here for two μ values only. The results for all μ used in this study are available on-line, for both electrons and ions (http://nis-www.lanl.gov/ friedel/pub/firstauthor/psa). The format of the plots in this section is the same as that described in section 4.1, with the addition of the Alfvén boundaries overplotted onto the data. The color bar represents the average flux observed in each bin. All boundaries are calculated by the same process as that used by *Korth et al.* [1999], using the electric and magnetic field models described in section 2. In the discussion that follows we further use the common locators noon, dawn, midnight and dusk, which correspond to GSM XY (15,0), (0,-15), (0,-15), and (0,15), respectively.

5.1. Electron Access

Plate 2 shows the results for electrons with μ = 1.0 $\mathrm{eV\ nT^{-1}}$ and Plate 3 shows the results for electrons with μ = 10.0 $\mathrm{eV\ nT^{-1}}$. Even a brief glance at Plates 2 and 3 reveals an agreement between the populated regions and the Alfvén boundaries that is remarkable, given the simple model and simple parameterization that these boundaries are based on.

A μ of 1.0 $\mathrm{eV\ nT^{-1}}$ (Plate 2) corresponds to an energy of ~ 125 eV at geosynchronous orbit. In general, electrons

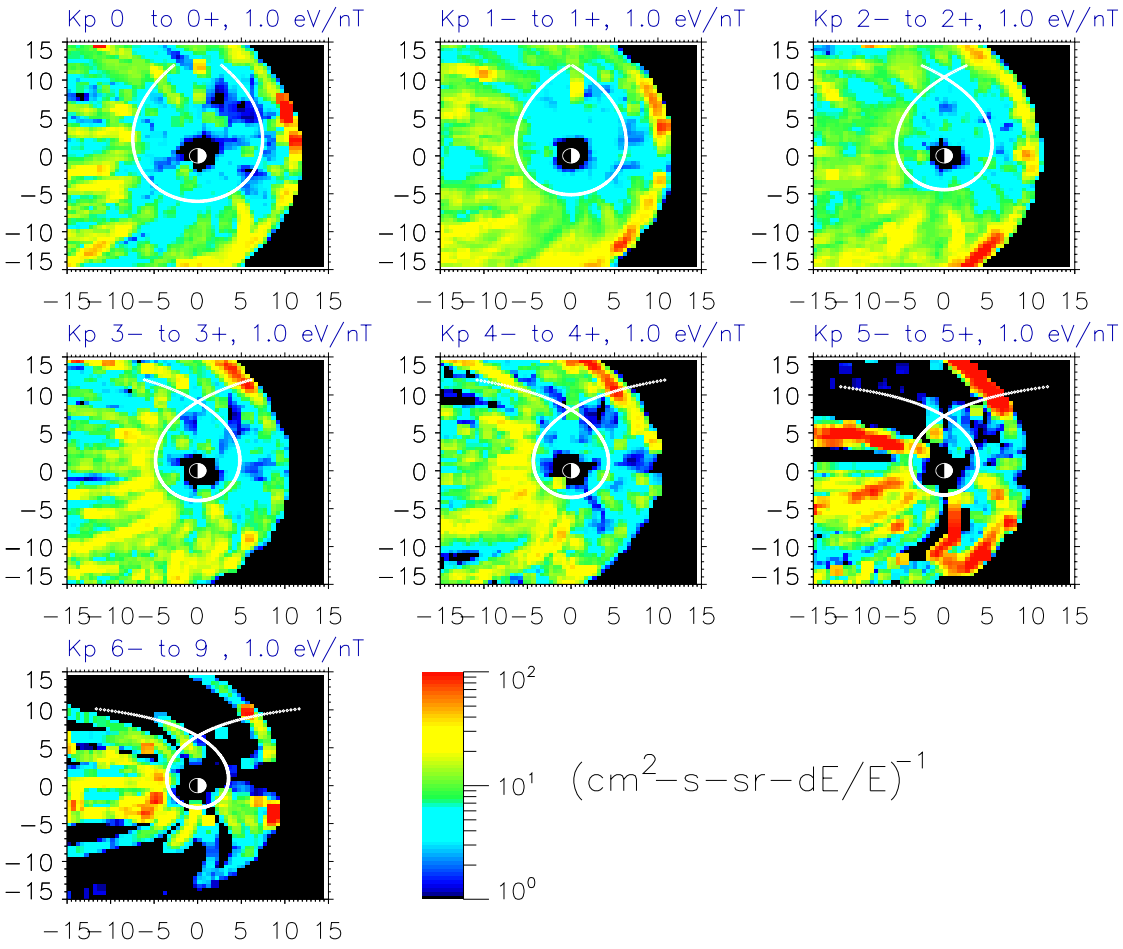

Plate 2. Average flux for electrons with μ = 1.0 eV nT^{-1}. See text for details.

convect in from the magnetotail from the midnight region, along equipotentials almost parallel to GSM $Y = 0$. As they enter the region where the Earth's corotational electric field starts dominating, they are deflected around the dawnside of the magnetosphere before drifting out toward the dayside magnetopause. On the duskside, at higher Kp, when the Alfvén boundary bulge moves further in, electrons can also flow around dusk.

At low Kp the inner edge of the Alfvén boundary is located near 6 R_E. At the low values of Kp, flux values are low globally, but any enhancements are seen only outside the Alfvén boundary. The region inside the Alfvén boundary becomes more and more depleted from noon to dusk, developing a deep minimum in that region. For these slowly convecting electrons, losses by wave-particle interaction are significant since they act over a long time.

As Kp increases, the Alfvén boundary shrinks, exhibiting more clearly the classic duskside bulge [*Lyons and Williams*, 1984]. Fluxes outside the Alfvén boundary are enhanced as convection increases with Kp, but there is always a distinct drop in fluxes as one crosses the boundary. On the dayside the region of electron depletion due to wave-scattering losses shrinks in local time: As electrons convect faster, they have a better chance of making it further around the dawnside before getting scattered and lost.

An interesting feature of the plots in Plate 2 is the enhancement of fluxes seen on field lines that map near the dayside magnetopause. These are electrons that enter the magnetosphere through the cusp. Their mapping around the dayside magnetopause is an artifact of the T87 model field lines near the cusp. This feature disappears for higher, non-solar wind μ (cusp energies are near $\sim$ 50 eV for electrons at magnetic field strengths near $\sim$ 10 nT, giving $\mu \sim 5$ eV nT^{-1} [*Fennell et al.*, 1998]).

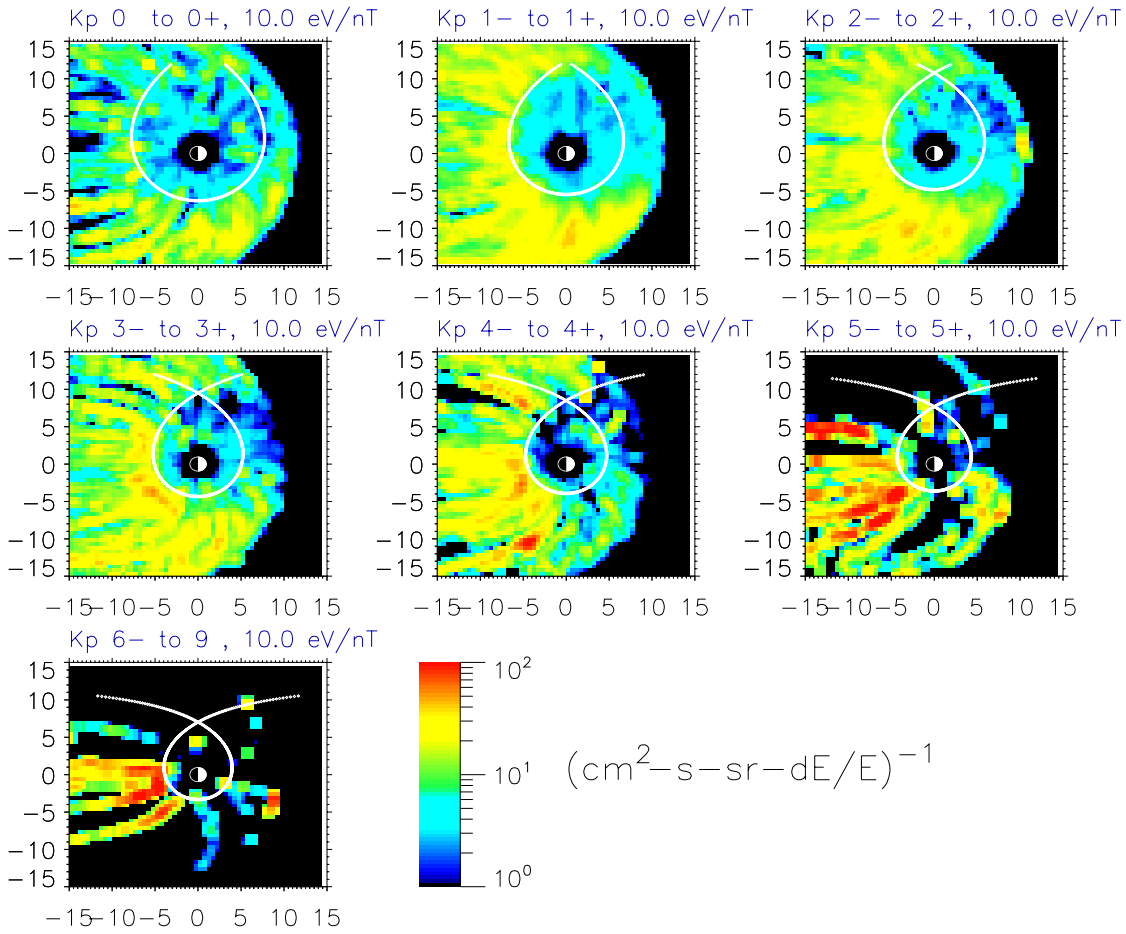

Plate 3. Average flux for electrons with μ = 10.0 eV nT^{-1}. See text for details.

A μ of 10.0 eV nT^{-1} (Plate 3) corresponds to an energy of $\sim$ 1 keV at geosynchronous orbit. The interpretation of these results is the same as for Plate 2, with the only difference being the position of the predicted Alfvén boundary, which for a higher μ is about $1.5R_E$ further out for all Kp. The agreement between the predicted Alfvèn boundary and access of electrons as shown in the data is again excellent.

5.2. Ion access

Plate 4 shows the results for ions with μ = 1.0 eV nT^{-1} and Plate 5 shows the results for ions with μ = 10.0 eV nT^{-1}. After the excellent data/model agreement obtained for electrons the results for ions were somewhat of a disappointment. Results in Plate 4 for 1.0 eV nT^{-1} ions show low, uniform flux throughout the tail region as well as the inner magnetosphere, with an organization of the data according to the Alfvén boundary becoming apparent at higher Kp only.

The low overall fluxes can have two causes. The first cause is that there never are many ions in this μ range in the plasma sheet. A value of 1.0 eV nT^{-1} corresponds to only $\sim$ 125 eV at geosynchronous altitudes, well below the average proton temperature of $\sim$ 7000 eV at geosynchronous altitude as measured by *Korth et al.* [1999]. The second cause is that losses occur at a rate faster than the average drift period of ions through the region. The ion Alfvén boundaries are very similar to the electron Alfvèn boundaries at this μ, as both species are dominated by the electric field drifts (see section 2.1), but there is an important difference. For electrons, electric field drifts and magnetic field drifts are always in the same direction. For ions these two drifts oppose. For low μ, electric field drifts predominate over the gradient and curvature magnetic field drifts, hence the same overall behavior of the boundaries as for electrons. However, the opposing gradient and curvature magnetic field drifts re-

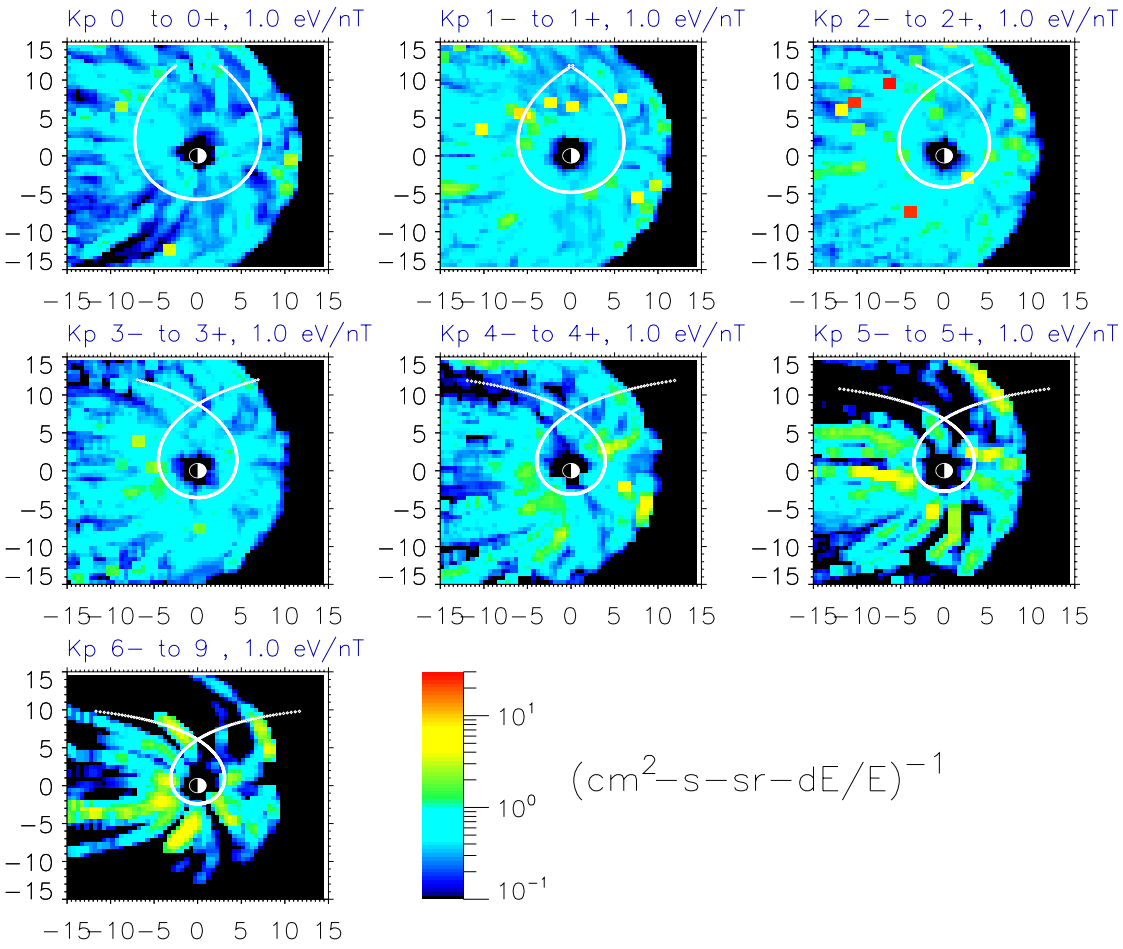

Plate 4. Results for 1.0 eV nT^{-1} ions. See text for details.

duce the ion drift velocity. So, especially for conditions of low convection (small Kp), ions spend a prolonged time in the inner region, exposed to the loss processes acting there. These loss processes, which for ions are mainly loss due to charge exchange, depend on a range of interaction cross sections which are all sensitive to the particle velocity: Low μ is slow, so these losses are high [*Fok et al.*, 1991]. All these effects may combine to wash out a visible particle boundary in the data for all but the largest Kp cases where convection due to the cross-tail electric field has increased significantly, thus increasing the ion drift velocity and allowing an Alfvén boundary to build up before losses can dominate.

A further complication is that HYDRA does not resolve ion composition: The data presented here are for total ions, all species. Drifts depend on particle charge state (see section 2), so that the drift paths for higher charge state ions (He^{++}, O^{++}) are very different and contribute to washing out of visible particle boundaries.

The scenarios become more complicated as we go up to a μ of 10.0 eV nT^{-1} shown in Plate 5. The Alfvén boundaries here show the transition between the stagnation point being at dusk (same as electrons) to being at dawn. The stagnation point is a point of zero drift, which for low-energy particles is at the point where the corotation and convection drifts balance at dusk. For ions, as Kp (convection drifts) increases, the combined ∇B and convection drifts overcome corotation at dusk, and ions start drifting westward. This westward drift can now form a new stagnation point at dusk where it opposes the convection drift. In the transition from one drift pattern to the other one can obtain complex "banana" orbits and multiple stagnation points [*Lyons and Williams*, 1984]. This behavior is analogous to increasing μ (∇B drift) and keeping Kp constant: This also leads to a transition of the stagnation point.

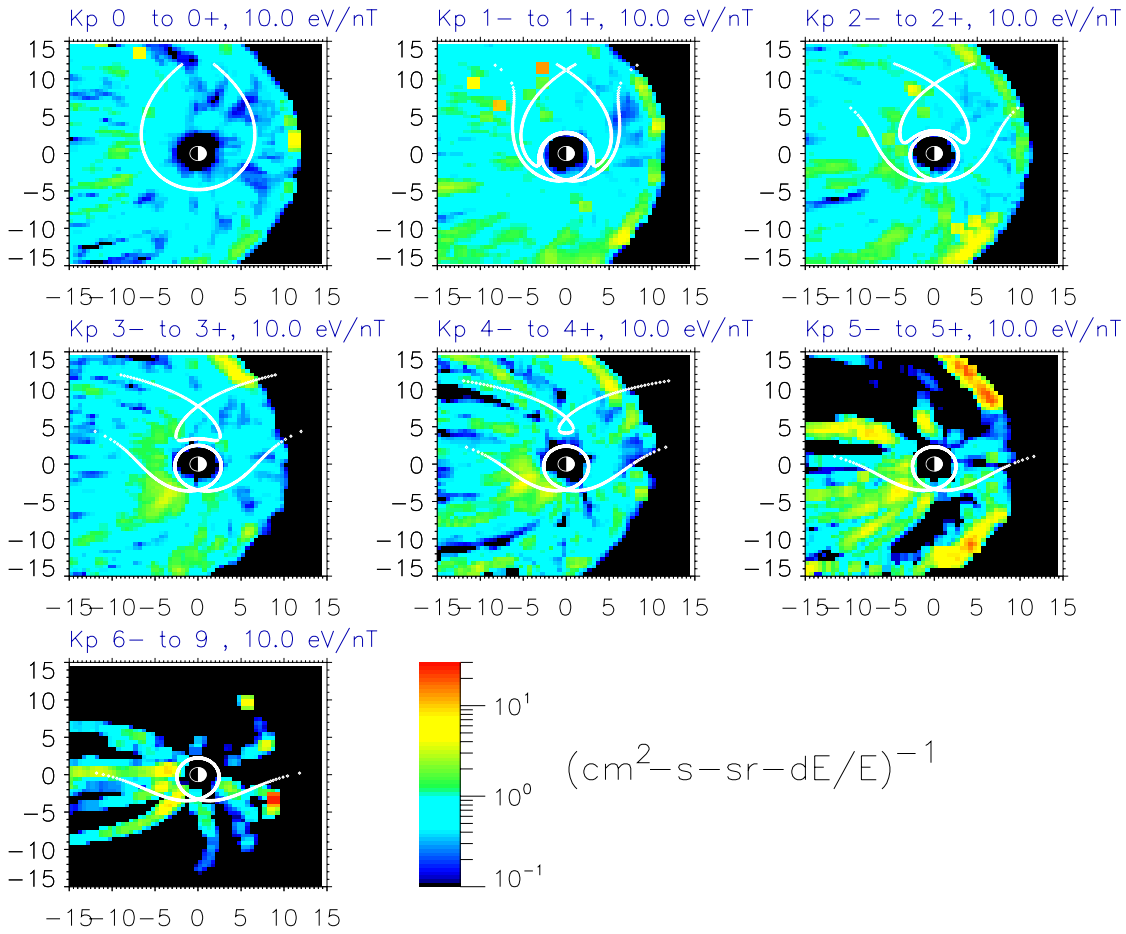

Plate 5. Results for 10.0 $\mathrm{eV\ nT^{-1}}$ ions. See text for details.

However, the agreement between the data and the inner, closed Alfvén boundary is quite good for all but the lowest Kp cases, for which the arguments above apply. Interesting to note is the very deep access of these ions compared to the same μ electrons.

5.3. Geosynchronous Comparison

In order to validate the HYDRA results in this study we can form a geosynchronous "slice" through our data and present it in an analogous form to the study by *Korth et al.* [1999]. This is a useful exercise not only as a consistency check but also to validate the many assumptions made in the analysis of Polar data and their mapping by μ to the equatorial plane. Plates 6 and 7 show the comparison between the results of *Korth et al.* [1999] and our study for electrons while the ion comparison is given in Plates 8 and 9.

The study by *Korth et al.* [1999] uses data from the plasma analyzer MPA [*McComas et al.*, 1993], which has been flown by Los Alamos National Laboratory on several concurrent satellites in geosynchronous orbit since 1989. The energy range for electrons and ions extends from $\sim$ 1 eV $\mathrm{q^{-}1}$ to $\sim$ 1 eV $\mathrm{q^{-}1}$. For their study a reduced data set of spin-averaged data from three satellites for the year 1996 was used.

The *Korth et al.* [1999] study (Plates 6 and 8) is limited to geosynchronous orbit (L near 6.6) and shows the results as a function of local time and Kp for various particle energies, which approximate to the same μ at all local times. This form of data display is useful in showing the range of local times that a particle of a given energy at that L has access to, for all Kp. The color plots for the various energies each have their own linear scaling.

The Polar HYDRA results (Plates 7 and 9) are for a slice through the data for $L = 6$ to 7 and are binned by magnetic

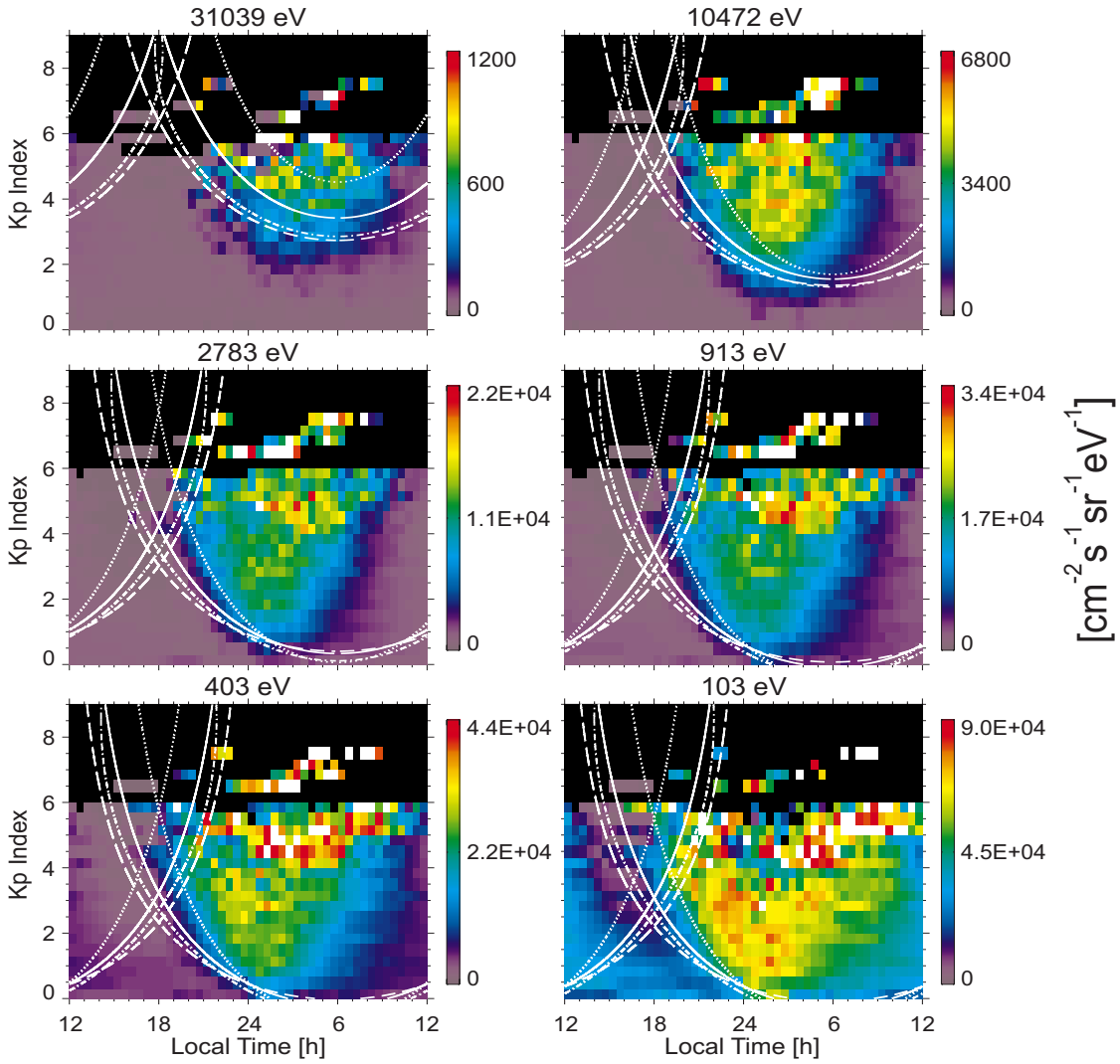

Plate 6. Geosynchronous electron results from *Korth et al.* [1999]. See text for details.

local time (MLT) using omni directional data. Since the energy channel assignment changes for HYDRA over time, we always interpolate the energy spectrum to a range of fixed energy channels. Fluxes are not corrected to the equator. All color plots use the same logarithmic scaling for each species.

The energy channels used by *Korth et al.* [1999] and in our study are slightly different. We show the results for the HYDRA channel nearest to the channels used by *Korth et al.* [1999] in the same position on the respective plots.

Even though the color scaling of the plots from *Korth et al.* [1999] and our plots differ, the actual boundaries in the data show up clearly. The intersections of the Alfvén layers with geosynchronous orbit for all Kp are shown on each plot. The white diamonds on the HYDRA plots correspond to the boundary calculation using the *Maynard and Chen* [1975] electric field model for a shielding exponent of $\gamma = 2$, which corresponds to the white dash-dot-dotted line in the *Korth et al.* [1999] plots.

In comparing the electron and ion results for both studies, several general comments can be made:

1. The agreement between the two data sets is excellent. Comparing each data set to the predicted Alfvén boundary shows the same degree agreement.

2. Even though the Polar measurements come from much higher magnetic latitudes (near 35^{o} for this time period) and the particles measured never have 90^{o} equatorial pitch an-

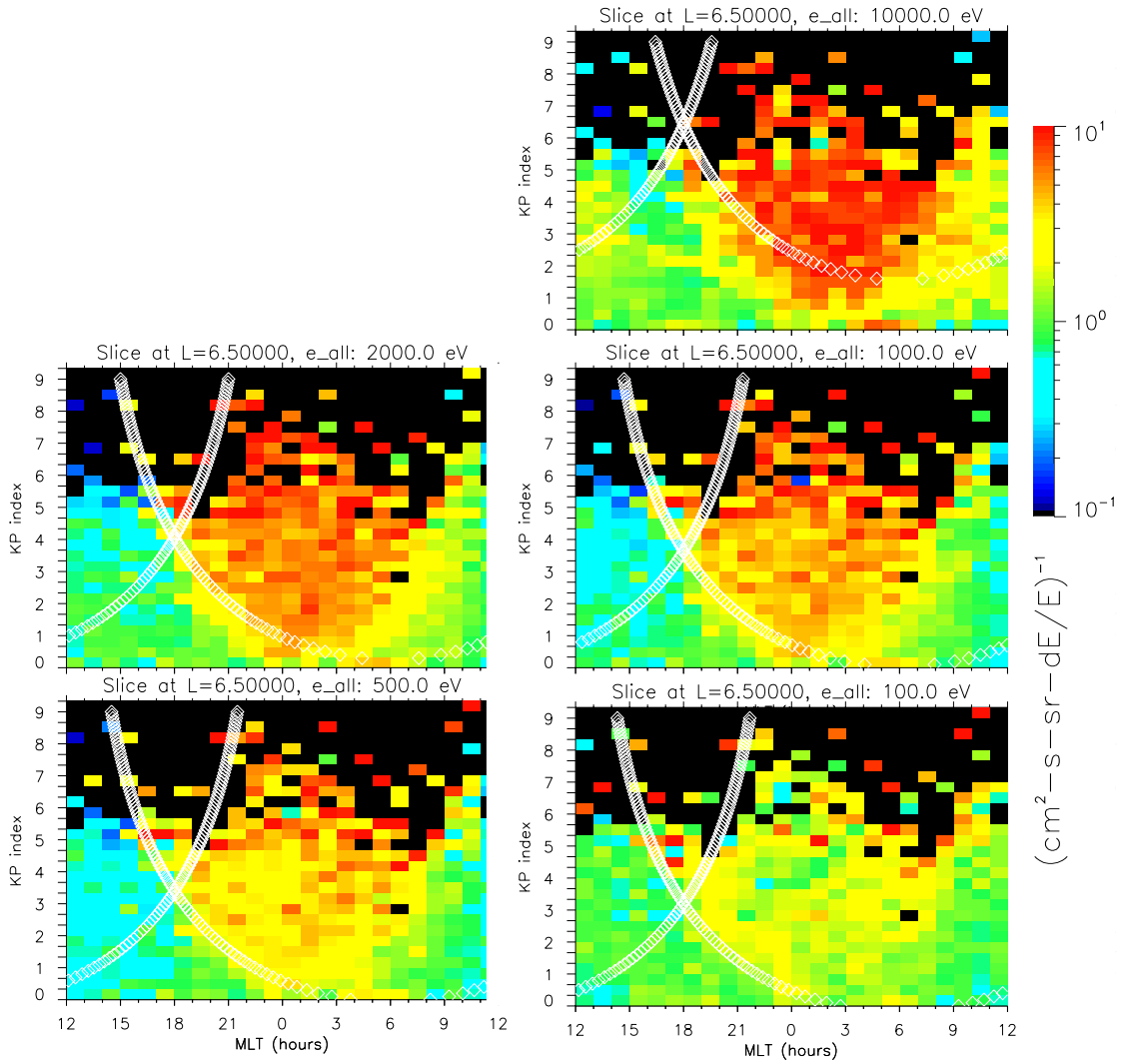

Plate 7. Geosynchronous slice from Polar HYDRA for electrons. See text for details.

gles, they organize in the same way as geosynchronous data do. This supports the assumption made in section 4.2 which uses the drift trajectories of 90^o equatorial pitch angle μ particles as representative for all pitch angles.

3. The Polar data show much more scatter compared to the geosynchronous data, which is no surprise given that the geosynchronous data are based on 1 year's worth of data (1996) from three different geosynchronous satellites ($\sim$ 1 million data points [*Korth et al.*, 1999]) while Polar crosses the geosynchronous L-shell 4 times an orbit or ~ 5500 times for the period considered here.

4. What is more of a surprise is that given the data density ratio of $\sim$ 180:1 between the two studies, that the Polar results match up to the geosynchronous results so well. There are thus enough Polar data to illuminate the trends. This indicates that the organization of the data by Alfvén layers is not only a statistical result that emerges by averaging a large number of data.

The geosynchronous results for the highest-energy electrons ($>$ 10 keV) in Plate 6 and 7 show a clear deviation between data and the predicted Alfvén boundaries. This has been attributed to an energy-dependent shielding exponent γ by [*Korth et al.*, 1999], which indicated that higher-energy channels are best fit by boundaries fit by the Gussenhoven $\gamma = 3$ model.

The geosynchronous results for the lowest-energy ions

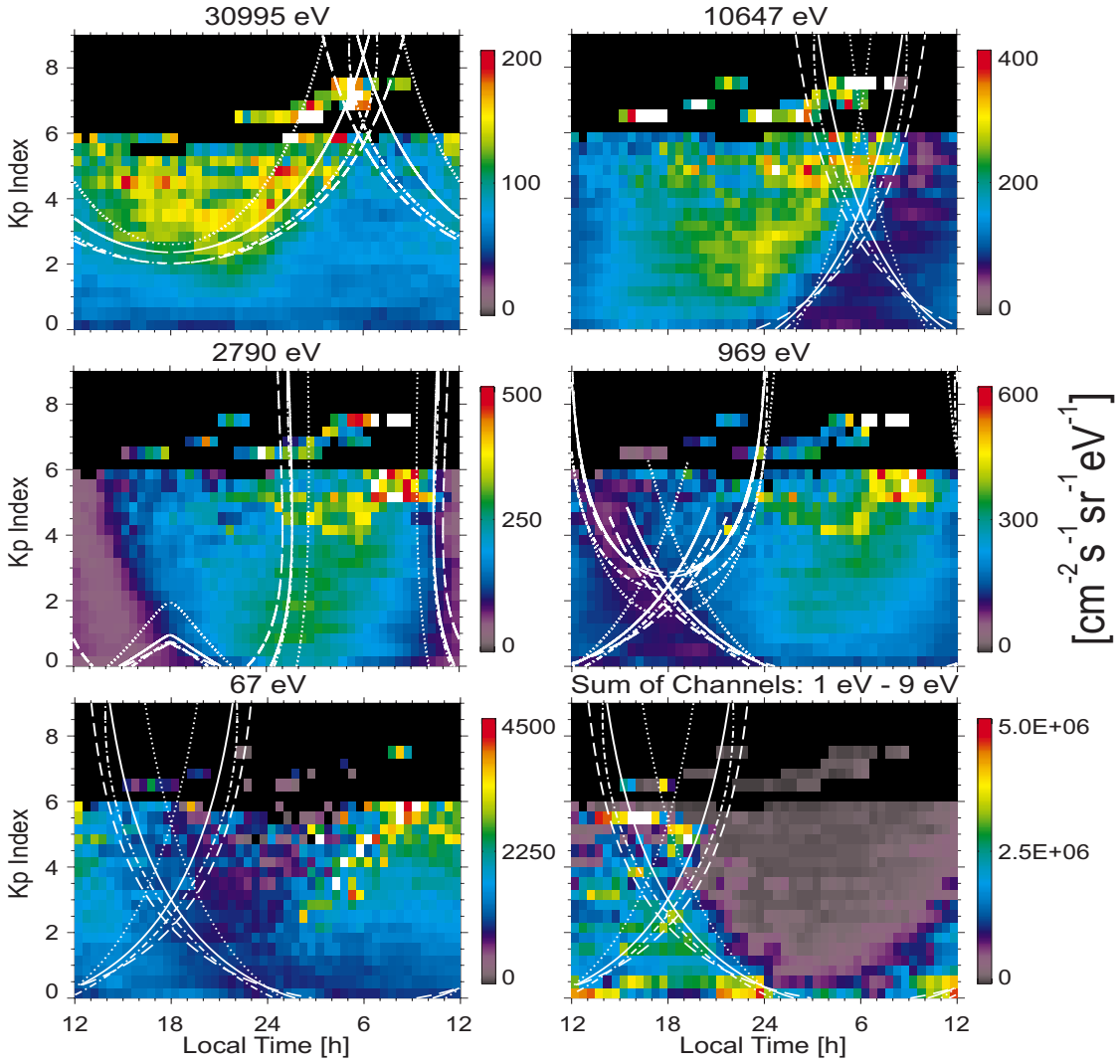

Plate 8. Geosynchronous ion results from *Korth et al.* [1999]. See text for details.

(1–9 eV) in Plate 8 show the opposite effect of where particles are present compared to higher energies: Low fluxes outside of the Alfvén boundary, high fluxes inside. This is due to a different source population for these energies (see section 2.2). These cold energies have their source in the ionosphere, and trapped orbits are needed for significant flux build up. HYDRA does not have the energy range to corroborate these results.

6. Summary

The Polar database is now large enough to provide comprehensive coverage of the plasma sheet particles in the inner magnetosphere below 15 R_E. We have shown here a statistical comparison of data to theoretically predicted plasma access boundaries in the inner magnetosphere. While the simple drift paradigm used here is one of the earliest pictures of particle motion in the Earth's magnetosphere, we have only now been able to test this paradigm thoroughly against data. The preceding study by *Korth et al.* [1999] explored the access conditions applied only to geosynchronous orbit. This study has expanded this test to the whole of the inner magnetosphere. We have shown excellent agreement for the experimental electron boundaries with the predicted Alfvén boundaries, and while the agreement for ions has not been as dramatic, the results can be understood in the framework of the same paradigm.

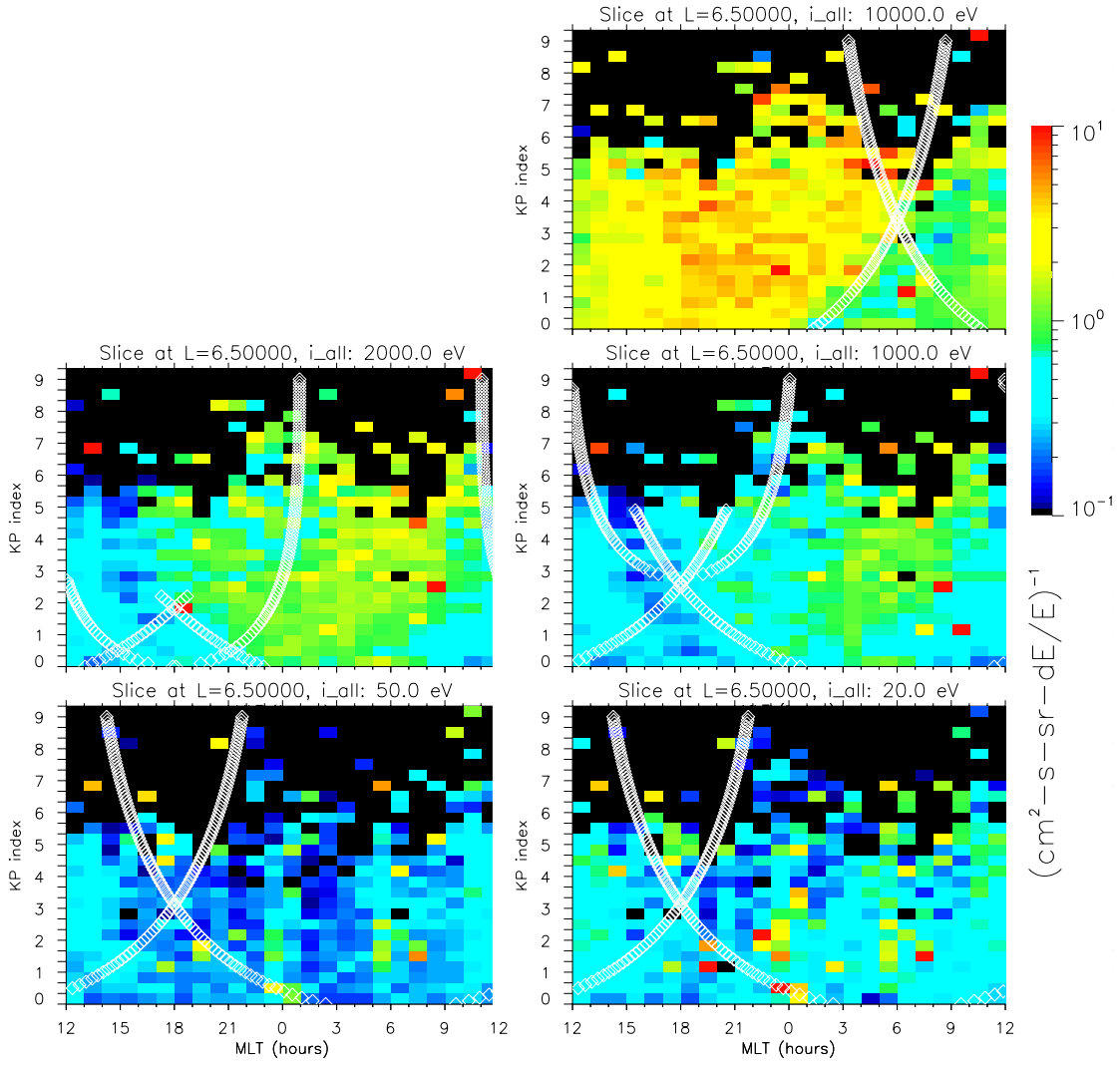

Plate 9. Geosynchronous slice from Polar HYDRA for ions. See text for details.

The results from Polar HYDRA have shown that electrons in the range of $\mu = 1-10\ \ nT/eV$ are sensitive tracers for the plasma access boundaries. The theoretical boundaries depend on both a magnetic and electric field model, so the data boundaries are a direct test for these models. Magnetic field models are a good representation of average magnetospheric conditions, since they are based on a large amount of data; the same cannot be said for electric field models. Taking the magnetic field models as "relatively good," this then makes the data boundaries observed and their fit to the predicted Alfvén boundaries a test of the electric field model used. The low μ used in this study are well suited for this, as electric field drifts predominate for these particles. Higher-energy particles are more sensitive to the magnetic field drifts, but this will be the subject of another paper.

While the simple corotation plus convection field model used here might not be able to describe detailed or localized field structures or their temporal evolution, it has certainly been shown that in a broad statistical sense the model is valid, and moreover, the simple parameterization of the cross-tail electric field by Kp found by *Maynard and Chen* [1975] is valid.

6.1. Electron Results

Electrons are very well organized by simple theoretical Alfvén boundaries. As μ decreases, electrons can penetrate

deeper into the magnetosphere. As Kp increases, the Alfvén boundaries move closer to Earth, also allowing deeper access. All μ show increasing losses as they drift toward the dayside. The longer the electrons drift, the more they can be lost by wave-particle interaction. At higher Kp particles have higher convection velocities and can drift around the dayside further, since they spend less time exposed to losses.

The Kp dependence of Alfvén boundaries agrees very well with data. Electron access is therefore primarily controlled by large-scale dawn-dusk electric fields, which in a statistical sense shows a simple dependence on Kp. The geosynchronous "slice" from HYDRA shows excellent agreement with the previous study using Los Alamos National Laboratory (LANL) geosynchronous data only but with poorer statistics due to the smaller database.

6.2. Ion results

The ion data, in general, do not organize as well Alfvén boundaries as the electron data. Ion drift orbits are more complex since $E \times B$ corotation and gradient/curvature drift effects are opposite. Low-energy particles have similar Alfvén boundaries compared to electrons but do not organize along this boundary: There seems to be fairly uniform access everywhere. This can be attributed to a combination of low plasma sheet fluxes in this μ range and the slow drift velocities of these ions (due to the opposing drifts), which means these ions spend a lot of time along their drift paths, so that losses can predominate over fresh access of new ions from the plasma sheet. Thus the Alfvén boundaries are not clearly visible, as losses have enough time to reduce the fluxes everywhere. Only at high Kp, or stronger convection, does fresh plasma from the plasma sheet organize along the Alfvén boundary.

Higher-energy ions show a transition of the stagnation point with Kp from dusk to dawn. Again, ions tend to be better organized by the Alfvén boundary for higher Kp.

The geosynchronous "slice" from HYDRA shows excellent agreement with previous study using LANL geosynchronous data only but with poorer statistics due to the smaller database.

All the ion data used here do not discriminate various ion species. As the drift path depends on the charge of the ion, higher charge state species (He^{++}, O^{++}) will have substantially different drift paths, which further mixes into the results obtained here.

6.3. Future Work

As the amount of data collected by Polar grows and Polar continues through the current solar maximum conditions, we will have the opportunity to increase our statistical coverage and to ask more detailed questions: How fast do the particles follow the boundaries on activity transitions (low $Kp \rightarrow$ high Kp and vice versa)? At each activity level, what is the quantitative loss rate of particles drifting through the magnetosphere? A further extension of this work is to include ion species in the same analysis, since Polar has excellent composition coverage over a wide energy range.

Acknowledgments. The HYDRA results of this paper are the results of NASA funding under grant NAG 5 2231 and German DARA funding under grant 50 OC 8911 0.

Janet G. Luhman thanks Petri Toivanen and Mei-Ching Fok for their assistance in evaluating this paper.

References

Abel, B., and R. M. Thorne, Electron scattering in earth's inner magnetosphere: 1. Dominant physical processes, *J. Geophys. Res.*, *103*, 2385–2396, 1998a.

Abel, B., and R. M. Thorne, Electron scattering in earth's inner magnetosphere: 2. Sensitivity to model parameters, *J. Geophys. Res.*, *103*, 2397–2407, 1998b.

Birn, J., M. F. Thomsen, J. E. Borovsky, G. D. Reeves, D. J. McComas, and R. D. Belian, Substorm ion injections: Geosynchronous observations and test particle orbits in three dimensional dynamic mhd fields, *J. Geophys. Res.*, *102*, 2325–2341, 1997.

Birn, J., M. F. Thomsen, J. E. Borovsky, G. D. Reeves, D. J. McComas, and R. D. Belian, Substorm electron injections: Geosynchronous observations and test particle simulations, *J. Geophys. Res.*, *103*, 9235–9248, 1998.

Bourdarie, S., D. Boscher, T.Beutier, J.-A. Sauvaud, and M. Blanc, Electron and proton radiation belt dynamic simulations during storm periods: A new asymmetric convection-diffusion model, *J. Geophys. Res.*, *102*, 17,541–17,552, 1997.

Fennell, J. F., J. L. Roeder, R. Friedel, M. Grande, and H. E. Spence, Dayside open field line region boundary at high altitudes , *Physics and Chemistry of the Earth*, *24*, 129–133, 1998.

Fok, M.-C., J. U. Kozyra, A. F. Nagy, and T. E. Cravens, Lifetime of ring current particles due to coulomb collisions in the plasmasphere, *J. Geophys. Res.*, *96*, 7861–7867, 1991.

Jordanova, V. K., et al., October 1995 magnetic cloud and accompanying storm activity: Ring current evolution, *J. Geophys. Res.*, *103*, 79–92, 1998.

Korth, A., R. H. W. Friedel, , C. G. Mouikis, J. F. Fennell, J. R. Wygant, and H. Korth, Comprehensive particle and field observations of magnetic storms at different local times from the CRRES spacecraft, *J. Geophys. Res.*, 2000, accepted.

Korth, H., M. F. Thomsen, J. E. Borovsky, and D. J. McComas, Plasma sheet access to geosynchronous orbit, *J. Geophys. Res.*, *104*, 25,047–25,061, 1999.

Lyons, L. R., and D. J. Williams, *Quantitative Aspects of Magnetospheric Physics*, 1st ed., D. Reidel Publishing Company, Dordrecht/Boston/Lancaster, 1984.

Maurice, S., M. F. Thomsen, D. J. McComas, and R. C. Elphic, Quiet time densities of hot ions at geosynchronous orbit, *J. Geophys. Res.*, *103*, 17,571–17,585, 1998.

Maynard, N. C., and A. J. Chen, Isolated cold plasma regions: Observations and their relation to possible production mechanisms, *J. Geophys. Res.*, *80*, 1975.

McComas, D. J., et al., Magnetospheric plasma analyzer (MPA): Initial three-spacecraft observations from geosynchronous orbit, *J. Geophys. Res.*, *98*, 13,453, 1993.

Roederer, J. G., *Dynamics of Geomagnetically Trapped Radiation*, Springer, New York, 1970.

Russell, C. T., R. C. Snare, J. D. Means, D. Pierce, D. Dearbourne, M. Larson, G. Barr., and G. Le, The GGS/POLAR magnetic field investigation, *Space Sci. Rev*, *71*, 563–582, 1995.

Scudder, J., et al., Hydra - a 3-dimensional electron and ion hot plasma instrument for the POLAR spacecraft of the GGS mission, *Space Sci. Rev*, *71*, 459–495, 1995.

Sheldon, R. B., and H. E. Spence, Alfven boundaries: Noses and zippers, *Adv. Sp. Res.*, *20*, 445–448, 1997.

Stern, D. P., Motion of a proton in the equatorial megentosphere, *J. Geophys. Res.*, *80*, 595–599, 1975.

Toivanen, P. K., T. I. Pulkkinen, R. H. W. Friedel, G. D. Reeves, A. Korth, C. Mouikis, and H. E. Koskinen, Time-dependent modeling of particles and electromagnetic fields during the substorm growth phase, *J. Geophys. Res.*, *103*, 10,205–10,220, 1999.

Volland, H. A., A semiempirical model of large scale magnetospheric electric fields, *J. Geophys. Res.*, *78*, 171–180, 1973.

Whipple, E. C., (U,B,K) coordinates: A natural system for studying magnetospheric convection, *J. Geophys. Res.*, *83*, 4318–4326, 1978.

Whipple, E. C., et al., Identification of magnetospheric particles that travel between spacecraft and their use to help obtain magnetospheric potential distributions, *J. Geophys. Res.*, *103*, 93–102, 1998.

Williams, D. J., The Earth's ring current: Present situation and future thrusts, *Phys. Scr.*, *T18*, 140–151, 1987.

R. H. W. Friedel, M. G. Henderson, H. Korth, and M. Thomsen, Los Alamos National Laboratory, Los Alamos, NM 87544. (friedel@lanl.gov)

J. D. Scudder, Deptartment of Physics and Astronomy, University of Iowa, Iowa City, IO 52242.

Received May 2, 2000 ; revised August 2, 2000; accepted August 29, 2000.